PCCP

PAPER

View Article Online
View Journal | View Issue

Cite this: *Phys. Chem. Chem. Phys.*, 2014, **16**, 14523

Predicting phosphorescent lifetimes and zero-field splitting of organometallic complexes with time-dependent density functional theory including spin–orbit coupling†

K. Mori,*[a] T. P. M. Goumans,[b] E. van Lenthe[b] and F. Wang[c]

Received 24th December 2013,
Accepted 11th March 2014

DOI: 10.1039/c3cp55438d

www.rsc.org/pccp

The (photo)physical properties of organometallic complexes are crucially affected by relativistic effects. In a non- or scalar-relativistic picture, triplet states are threefold degenerate. Spin–orbit coupling lifts this degeneracy (zero-field splitting, ZFS) and enables phosphorescence from the three triplet-like states to the ground state. The fine structure and radiative lifetimes of phosphorescent organometallic complexes are important properties for designing efficient organic light-emitting diodes (OLEDs). Here we show that experimental ZFSs and phosphorescent lifetimes for a large variety of organometallic complexes are well reproduced by self-consistent spin–orbit coupling TDDFT (SOC-TDDFT) calculations with a continuum solvation model. By comparing with perturbative SOC-TDDFT and gas phase calculations, we find that both full spin–orbit and solvation effects are important for the predicted properties. SOC-TDDFT is thus shown to be a useful predictive tool for the rational design of phosphors in OLEDs and other optoelectronic devices.

1. Introduction

The photophysical properties of organometallic complexes are intensively studied from experimental and theoretical perspectives because of their important applications. Tweaking light absorption and emission properties of these complexes is essential for optimizing the efficiency of optoelectronic devices such as organic light-emitting diodes (OLEDs)[1–4] and dye-sensitized solar cells (DSSCs).[5] Likewise, photochemical properties of organometallic complexes are important for other applications such as (bio)-chemical sensing[6] and photoredox catalysis.[7]

The organometallic complexes that are most efficient for these applications typically contain transition metals with 4d and 5d electrons, more specifically the platinum group metals (Ru, Rh, Pd; Os, Ir, Pt). For these heavy elements major relativistic effects are in play.[8,9] While scalar relativistic or pseudo-relativistic corrections are often, but not always, sufficient to accurately describe geometries, a relativistic picture that includes the spin–orbit interaction can significantly affect spectroscopic properties.[9] Particularly, spin–orbit coupling (SOC) induces fast intersystem crossing (ISC) and phosphorescent decay in organometallic complexes, which makes them suitable for applications in high-efficiency OLEDs.[10,11]

In purely organic materials, electroluminescence typically occurs from singlet excitons, comprising only one quarter of the hole–electron recombination events. The triplet excitons in such materials are wasted as heat through triplet–triplet recombination and other non-radiative decay pathways. Thus, OLED efficiency can be greatly enhanced by harvesting triplet excitons.[2] Fast ISC in organometallic complexes induced by SOC can increase the theoretical maximum luminescence quantum yield from 25% to 100%. For high-efficiency OLEDs, the triplet states of these compounds should have high radiative rates to compete with non-radiative deactivation pathways. The discovery of efficient red[10] and green[11] emitting phosphors by the Forrest group spurred research to further develop phosphorescent OLED materials for energy efficient lighting and electronics solutions as well as the promising application of eco-friendly, flat, and flexible displays. The realization of a stable and high-efficiency blue-emitting organometallic phosphor is particularly challenging.[12]

At the scalar relativistic (or pseudo-relativistic) level $S_0 \rightarrow T_1$ absorption and $T_1 \rightarrow S_0$ emission are strictly spin-forbidden, but SOC mixes singlet and triplet states, enabling these processes. Therefore, to rationally design new and better organometallic phosphors for OLEDs, accurate theoretical methods that can treat excited states with SOC are necessary. On the other hand,

[a] *Ryoka Systems Inc., Science and Technology Systems Division, Tokyo Skytree East Tower 1-1-2, Oshiage, Sumida-ku, Tokyo 131-0045, Japan. E-mail: mori@rsi.co.jp*
[b] *Scientific Computing & Modelling NV, Theoretical Chemistry, Vrije Universiteit, De Boelelaan 1083, 1081 HV Amsterdam, The Netherlands*
[c] *College of Chemistry, Sichuan University, 24, South Section 1, Yihuan Road, Chengdu, 610064 Sichuan, P. R. China*

† Electronic supplementary information (ESI) available. See DOI: 10.1039/c3cp55438d

while a multi-reference *ab initio* method such as CASPT2 with a carefully selected active space may be feasible for a few selected (model) compounds, practical applications to large-size organometallic complexes require fast and robust methods such as density functional theory (DFT).

Since the influential discovery of high phosphorescence efficiency of Ir complexes,[11,13] these are often used in OLEDs. A decade ago, Hay demonstrated that time-dependent DFT (TDDFT) can accurately model excited states of Ir complexes.[14] However, important phosphorescent properties such as zero-field splitting (ZFS) and emission lifetimes can only be modeled in a relativistic framework that includes spin–orbit interactions at the TDDFT level.[15–20]

For tractable relativistic calculations on sizeable chemical systems the four-component Dirac or Dirac–Kohn–Sham equations are often reduced by an expansion in leading terms of order $1/c^2$. The zero order regular approximation (ZORA)[21,22] expands the Dirac equation in $E/(2c^2 - V)$, and contains corrections in $1/c^2$ to all orders. The ZORA Hamiltonian can be written as the sum of a scalar relativistic (SR) part and a SOC part:

$$H^{\mathrm{ZORA}} = H^{\mathrm{SR}} + H^{\mathrm{SOC}} \quad (1)$$

With this partitioning, SOC can be included self-consistently during the SCF and TDDFT calculations (SOC-TDDFT).[23] Alternatively, SOC can be included as a perturbation based on the scalar relativistic orbitals (pSOC-TDDFT).[24] As with other perturbative approaches, pSOC-TDDFT is best applied to systems where the perturbation (SOC) is small. While full SOC-TDDFT is theoretically a more accurate approach, it is more computationally demanding than pSOC-TDDFT for the same number of excitations.

In several recent papers the photophysical properties of typical Ir complexes have been successfully studied with (p)SOC-TDDFT.[3,4,19,20,25] By switching on SR and SOC effects gradually in the calculations, the impact on (photo)physical properties of both effects were shown to be of vital importance.[19,20] The SR corrections expand the 5d orbitals of the central Ir atom, stabilizing the triplet metal to ligand charge transfer state (^{3}MLCT), which in turn further facilitates singlet–triplet mixing through SOC.

On the other hand, calculations of phosphorescent properties with (p)SOC-TDDFT have not yet been reported for a varied set of large-sized complexes with central transition metals spanning the platinum group metals. Therefore, an extensive study is still required to validate the accuracy of these methods by comparing predicted ZFS and phosphorescent lifetimes to available experimental data. Furthermore, the impact of solvation in the computational model, which will be shown to be important in this work, has not been comprehensively investigated along these lines.

In this paper we report ZFS and radiative lifetime calculations for the triplet state of a large number of 4d and 5d organometallic complexes, using (p)SOC-TDDFT and a continuum solvation model.

The results are presented as follows: first, we describe our computational details for calculating ZFS and radiative lifetime. In the next section, we compare our best theoretical results (SOC-TDDFT with a continuum solvation model) to experimental data. The impact of full spin–orbit and solvation effects is then demonstrated by comparing with pSOC-TDDFT and the gas phase calculations, respectively. Finally, we compare our results for a typical Ir compound $Ir(ppy)_3$ to earlier theoretical studies employing other perturbative SOC approaches.

2. Computational details

SOC-TDDFT[23] and pSOC-TDDFT[24] calculations with the ZORA Hamiltonian[21,22] were performed with ADF2013.[26,27] The B3LYP[28] hybrid exchange–correlation functional was used with all electron Slater-type orbital basis sets:[29] triple-zeta + polarization (TZP) for the central transition metal and double-zeta + polarization (DZP) for all other atoms. The SR-TDDFT calculations included 20 singlet + 20 triplet excitations, which are used as the basis for the perturbative expansion in the pSOC-TDDFT calculations. Perturbative SOC corrections were also applied to the ground state. At least 4 spin-mixed excitations were calculated in the full SOC-TDDFT calculations, where the SR-TDDFT result was used as an input, with which the singlet and triplet contributions to the spin-mixed excitations[30] were confirmed. The following technical settings were employed: Becke numerical integration grids of "Good" quality,[31] ExactDensity, SCF convergence of 1×10^{-6} Hartree, gradients convergence of 1×10^{-4} Hartree per Å for geometry optimization.

Lowest triplet states were optimized by specifying two unpaired electrons (unrestricted DFT) in a regular geometry optimization with the SR ZORA Hamiltonian with lowered symmetry, because the triplet excited state breaks the D_3 (or C_3) symmetry of symmetric octahedral complexes through the Jahn–Teller effect.[32]

Environmental effects were included *via* COSMO continuum solvation[33] using dichloromethane parameters while a range of media were used in available experimental data. For the pSOC-TDDFT calculations, the effect of the excitations on the COSMO surface charges of the excitations was not taken into account. In the fully self-consistent SOC-TDDFT calculations, the change in COSMO surface charges was taken into account for the spin-mixed excitations.

The radiative rate k_i and radiative lifetime τ_i from substate i (i = 1, 2, 3) of the T_1 state to the ground state were calculated from the excitation energy ΔE_i and the transition dipole moment $\mathbf{M}^i$ with SOC included:

$$k_i = \frac{1}{\tau_i} = \frac{4}{3t_0}\alpha_0{}^3(\Delta E_i)^3 \sum_{\alpha\in\{x,y,z\}} \left|M_\alpha^i\right|^2 \quad (2)$$

with $t_0 = (4\pi\varepsilon_0)^2\hbar^3/m_e e^4$ and α_0 the fine structure constant. In a medium, these are corrected for the refractive index n according to the Strickler–Berg relationship.[15,34] According to this correction, our calculated radiative rate k_i (or radiative lifetime τ_i) was multiplied (or divided) by the square of the refractive index of dichloromethane (n = 1.42).

The observed radiative lifetime is then an average over the three substates under the assumption of fast thermalization:

$$\tau_{av} = \frac{1}{k_{av}} = \left(\frac{3}{k_1 + k_2 + k_3}\right) \quad (3)$$

or, more accurately, a Boltzmann average when the energy difference between the T_1 substates is non-negligible with respect to the temperature T:

$$\tau_{av} = \frac{1}{k_{av}} = \left(\frac{1 + e^{-(\Delta E_{1,2}/k_B T)} + e^{-(\Delta E_{1,3}/k_B T)}}{k_1 + k_2 e^{-(\Delta E_{1,2}/k_B T)} + k_3 e^{-(\Delta E_{1,3}/k_B T)}}\right) \quad (4)$$

with k_B the Boltzmann constant. Eqn (4) at T = 300 K was used for our calculated lifetimes.

The ZFS was calculated as the energy difference between the highest and the lowest substates of the T_1 state. The triplet state is typically split into three substates, except for calculations with D_3 (or C_3) symmetry constraint, where the T_1 state splits into an A_1 (or A) and a degenerate E state. As mentioned above, the Jahn–Teller effect will lift the degeneracy of the E state by lowering the symmetry to C_2 (or C_1).

3. Results and discussion

23 organometallic complexes, for which experimental ZFS and radiative lifetimes have been determined, were studied with (perturbative) SOC-TDDFT, both in the gas phase and with the COSMO continuum solvation model. The broad set contains various transition metals and ligands.

3.1 COSMO + SOC-TDDFT in comparison with experiment

Table 1 summarizes our best theoretical calculations (COSMO + SOC-TDDFT) and compares them to experimental data, which were predominantly taken from a recent review by Yersin *et al.*[2] The experimental ZFSs span a range from nearly 0 to over 150 cm^{-1} in the **23** compounds, while the radiative decay times τ^r span more than three orders of magnitude. A higher ZFS originates from a stronger SOC, which means that at least one triplet substate has a larger singlet character, leading to a higher oscillator strength for emission to the ground state. A high radiative rate (short radiative lifetime) is desirable for application in high-efficiency OLEDs.

The triplet states of the **23** compounds are grouped into three classes according to the ordering scheme by Yersin based on the experimental ZFS magnitude.[1,2] Complexes (**1–5**) with ZFS <4 cm^{-1} are classified as ligand centred (^{3}LC) and complexes (**14–23**) with ZFS exceeding 50 cm^{-1} as ^{3}MLCT states. Complexes (**6–13**), with an intermediate ZFS, are classified as a mixed ^{3}LC/^{3}MLCT state. These classifications are listed in Table 1.

The COSMO + SOC-TDDFT data are in very close agreement with the experimental data, as visualized in Fig. 1. The majority of calculated ZFS values are in excellent agreement with experiment, either within the reported range or within ± 10 cm^{-1} of the highest value. Four predicted ZFSs are notably higher: Ir(s1-thpy)$_2$(acac) (**11**) from the compounds with ^{3}LC/^{3}MLCT character, and $[Ru(bpy)_3]^{2+}$, Ir(biqa)$_3$ and Ir(pbt)$_2$(acac) (**16**, **17**, **19**) from the ^{3}MLCT group. These ZFS values are larger than the highest reported value by 19, 61, 40, and 78 cm^{-1}, respectively.

The calculated τ^r values clearly reproduce the experimental trend in which the radiative lifetime decreases by more than three orders of magnitude from the ^{3}LC to ^{3}MLCT states (note the logarithmic scale for τ^r in Fig. 1). The calculated τ^r values are in good agreement with experiment (within about $\pm$50%), with the exception of $[Rh(bpy)_3]^{3+}$ (**1**), with ^{3}LC character, and the mixed ^{3}LC/^{3}MLCT compound Pt(thpy)$_2$ (**10**). The calculated τ^r for these compounds is relatively large: 4.7 and 2.7 times larger than the experiment, respectively.

The least accurate prediction in our data set of 23 complexes is for the slowest triplet emitter, $[Rh(bpy)_3]^{3+}$ (**1**), with the calculated radiative lifetime being 4.7 times longer than the experimental emissive decay time. The lifetime of (**1**) exceeds a millisecond, which makes competition by non-radiative decay pathways likely. This in turn reduces the measured emission decay time with respect to the actual radiative lifetime:[2]

$$\tau_{emission} = \frac{\Phi_{PL}}{k^r} = \frac{1}{k^r + k^{nr}} \quad (5)$$

with Φ_{PL} the emission quantum yield, k^r and k^{nr} the radiative and non-radiative rates. Likewise, for other complexes where no quantum yield has been determined (**2**, **3**, **5**), the lower measured emission decay times compared to our calculated values could be due to competitive non-radiative processes.

For the triplet states, lower-symmetry geometries (C_1, C_2) were preferred energetically for most complexes we studied, as shown in Table 1, while the singlet ground states had higher symmetries (C_2, C_3, D_3). The symmetry of an organometallic complex can severely affect the ZFS and τ^r, so we also calculated the values at T_1 geometries with higher symmetry constraints, which are reported within brackets for selected compounds (**3**, **10**, **16**, **21**, **23**).

The most notable effect of the molecular symmetry of the T_1 state is seen for the complexes $[Ru/Os(bpy)_3]^{2+}$ (**16**/**23**), which are D_3 symmetric in their S_0 states. Nozaki *et al.* noted that the lowest ^{3}MLCT state of $[Os(bpy)_3]^{2+}$ (**23**) varies with the environment: delocalized D_3 in PF_6 salt, partially localized C_2 in glass matrix, fully localized C_2 in solution.[32] Consequently, our calculated data at the COSMO + SOC-TDDFT level are in good agreement by considering the symmetries depending on the experimental environments. The ZFS at the D_3 geometry (shown in brackets in Table 1) compares favorably to the highly resolved spectrum of $[Os(bpy)_3]^{2+}$ doped in $[Ru(bpy)_3](PF_6)_2$ salt (181 cm^{-1} *vs.* 217 cm^{-1}), although τ^r at D_3 symmetry (0.6 μs) is much shorter than the experimental values observed in the PMMA glass matrix (26.1 μs) and in acetonitrile solution (12 μs). τ^r at D_3 symmetry is slightly closer to the ethanol/methanol glass matrix value for $[Os(4,4'\text{-}Me_2bpy)_3]^{2+}$ (5.1 μs) which is reportedly[15] more accurate than that of $[Os(bpy)_3]^{2+}$ in PMMA. As a check, we confirmed that the calculated photophysical properties are nearly identical for both these similar Os complexes.

On the other hand, the τ^r calculated at C_2 symmetry (5.9 μs) is in excellent agreement with the $[Os(4,4'\text{-}Me_2bpy)_3]^{2+}$ value although the ZFS at C_2 symmetry (691 cm^{-1}) is significantly

Table 1 Calculated ZFS (cm^{-1}) and radiative lifetime τ^r (μs) of COSMO + SOC-TDDFT compared to experimental data. Experimental τ^r within parentheses are emission decay times. The radiative decay time cannot be given because the emission quantum yield is not available. Calculated values within brackets are ZFS and τ^r at T_1 geometries constrained to the higher symmetries of the S_0 states

No.	Compound[a]	Symmetry change from S_0 to T_1	ΔE(ZFS) [cm^{-1}]		τ^r (300 K) [μs]		Classification	Ref.
			Calc.	Exp.	Calc.	Exp.		
1	$[Rh(bpy)_3]^{3+}$	$D_3 \rightarrow C_2$	0.1	0.04[b,c] 0.077[b,c] 0.116[b,c]	5.6×10^3	$(1.2 \times 10^3$[b,d])	^{3}LC	2
2	$[Ir(bpy)_3]^{3+}$	$D_3 \rightarrow C_2$	1.6		87.1	(54[e,f])	^{3}LC	35
3	$Pd(thpy)_2$	$C_2 \rightarrow C_1$	0.9 [6.6]	0.0962[c,g]	287.8 [50.0]	(235[d,g])	^{3}LC	2
4	Pt(s1-thpy)(acac)	C_1	4.5	<1[g,h]	47.5	56[g,i] 49[i,j]	^{3}LC	2
5	$Re(pbt)(CO)_4$	C_1	1.3	<2[h,k]	78.0	(65[d,k])	^{3}LC	2
6	Pt(thpy)(acac)	C_1	5.8	4.3[g,h]	38.7	35[g,i] 38[i,j]	^{3}LC/^{3}MLCT	2
7	Pt(4,6-dFpthiq)(dpm)	C_1	9.7	6[g,h] 6[j,l]	14.3	18[i,j] 14[i,j]	^{3}LC/^{3}MLCT	2
8	Pt(4,6-dFppy)(acac)	C_1	14.9	8.3[g,h]	11.3	10.0[i,m] 10.6[i,j]	^{3}LC/^{3}MLCT	2
9	Pt(pbt)(acac)	C_1	13.1	10[h,n]	15.9	16.7[i,j]	^{3}LC/^{3}MLCT	2
10	$Pt(thpy)_2$	$C_2 \rightarrow C_1$	13.6 [52.0]	16[g,h]	20.0 [6.1]	7.3[i,o]	^{3}LC/^{3}MLCT	2
11	$Ir(s1\text{-}thpy)_2(acac)$	C_2	34.5	16[h,k]	10.1	14.1[i,k] 10.2[i,j]	^{3}LC/^{3}MLCT	2
12	$Ir(btp)_2(acac)$	$C_2 \rightarrow C_1$	17.7	14.8[h,k,p] 25[h,k,p]	25.4	29.0[i,m]	^{3}LC/^{3}MLCT	2
13	$Ir(thpy)_2(acac)$	C_2	38.0	34[h,k]	8.0	16.8[i,k] 8.7[i,j]	^{3}LC/^{3}MLCT	2
14	$Ir(4,6\text{-}dFppy)_2(pic)$	C_1	53.6	41–66[l,q,r] 76[h,k]	3.2	2.1[i,q] 2.3[i,k]	^{3}MLCT	2
15	$Ir(piq)_3$	$C_3 \rightarrow C_1$	71.8	43–57[k,l,r] 64[j,l]	3.4	2.3[i,k] 2.8[i,m]	^{3}MLCT	2
16	$[Ru(bpy)_3]^{2+}$	$D_3 \rightarrow C_2$	122.0 [31.4]	61[b,h]	4.9 [3.0]	15.0[i,s,t] 9.8[i,s,t]	^{3}MLCT	2, 36
17	$Ir(biqa)_3$	$C_3 \rightarrow C_1$	118.2	78[l,m]	1.5	1.3[m,u]	^{3}MLCT	2
18	$Ir(piq)_2(acac)$	$C_2 \rightarrow C_1$	95.7	96[l,q]	3.4	5.5[i,q,v]	^{3}MLCT	2
19	$Ir(pbt)_2(acac)$	$C_2 \rightarrow C_1$	181.0	103[g,l]	2.8	6.9[i,m]	^{3}MLCT	2
20	$Ir(4,6\text{-}dFppy)_2(acac)$	$C_2 \rightarrow C_1$	124.0	80–125[l,q,r] 109[h,k]	1.9	1.8[i,q] 1.6[i,k]	^{3}MLCT	2
21	$Ir(dm\text{-}2\text{-}piq)_2(acac)$	$C_2 \rightarrow C_1$	168.3 [134.7]	150–160[k,l,r]	2.1 [1.1]	2.1[i,k,w]	^{3}MLCT	2
22	$Ir(ppy)_3$	$C_3 \rightarrow C_1$	105.3	85–150[l,q,r] 114–135[j,l,r] 170[h,k]	2.1	1.6[i,m] 1.45[j,u] 1.8[i,k]	^{3}MLCT	2
23	$[Os(bpy)_3]^{2+}$	$D_3 \rightarrow C_2$	690.5 [180.7]	52[j,l] 134[f,l,x] 217[h,y]	5.9 [0.6]	26.1[j,u] 5.1[f,u,x] 12[i,z]	^{3}MLCT	37–39

[a] Abbreviation for ligands: bpy = 2,2′-bipyridinate; thpy = 2-(2′-thienyl)pyridinate; s1-thpy = 5-phenyl-2-(2-thienyl)-cyclopenteno[*c*]pyridinate; acac = acetylacetonate; pbt = 2-phenylbenzothiazolate; 4,6-dFpthiq = 2-(4′,6′-difluorophenyl)tetrahydroisoquinolinate; dpm = dipivaloylmethanate; 4,6-dFppy = 2-(4′,6′-difluorophenyl)pyridinate; btp = 2-(2′-benzothienyl)-pyridinate; pic = picolinate; piq = 1-phenylisoquinolinate; biqa = 6-[*t*]butyl-benzimidazo[1,2*c*]quinazolinate; dm-2-piq = 2-(3,5-dimethylphenyl)quinolinate; ppy = phenylpyridinate. [b] Measured in $[Zn(bpy)_3](ClO_4)_2$. [c] From ODMR measurements. [d] Calculated by use of the three individual emission decay times and of the zero-field splitting values according to eqn (4) for a temperature of 300 K. [e] From emission decay time measurements at low temperatures. [f] Measured in ethanol/methanol. [g] Measured in *n*-octane. [h] From highly resolved spectra. [i] Calculated from the emission quantum yield and the decay time measured at ambient temperature according to eqn (5). [j] Measured in PMMA. [k] Measured in CH_2Cl_2. [l] From a fitting procedure. [m] Measured in 2-MeTHF. [n] Measured in *n*-hexane. [o] Measured in butyronitrile. [p] Different site. [q] Measured in THF. [r] Inhomogeneous distribution. [s] Measured in toluene/ethanol/methanol. [t] The emission quantum yield was measured in acetonitrile. [u] Calculated by use of the three individual radiative decay times and of the zero-field splitting values according to eqn (4) for a temperature of 300 K. [v] The emission quantum yield was measured in CH_2Cl_2. [w] The emission quantum yield was measured in PMMA. [x] $[Os(4,4'\text{-}Me_2bpy)_3]^{2+}$. [y] Measured in $[Ru(bpy)_3](PF_6)_2$. [z] Measured in acetonitrile.

larger than the experimental values in salt and glass matrices. The calculated τ^r at C_2 symmetry also compares well with the value in acetonitrile (5.9 μs *vs.* 12 μs). The values which agree best have been used in Fig. 1.

Qualitative considerations: Ir(III) and Pt(II) complexes. Most extensive data are available for Ir(III) and Pt(II) complexes in our data set of 23 complexes. As seen from Table 1 (and visualized in Fig. S1 in the ESI†), octahedral Ir(III) complexes with bridging N^C ligands typically show the largest ZFS and radiative rates (shortest phosphorescent lifetimes), while square-planar Pt(II) complexes show much lower ZFS and longer-lived triplet states, despite a comparable SOC constant on the transition metal.[2] This behavior can be qualitatively explained in a ligand field/frontier molecular orbital picture using degenerate/second order perturbation theory.[1,2]

Typically, the lowest excited states in a strong field are triplet metal-to-ligand charge transfer states (^{3}MLCT), where an electron

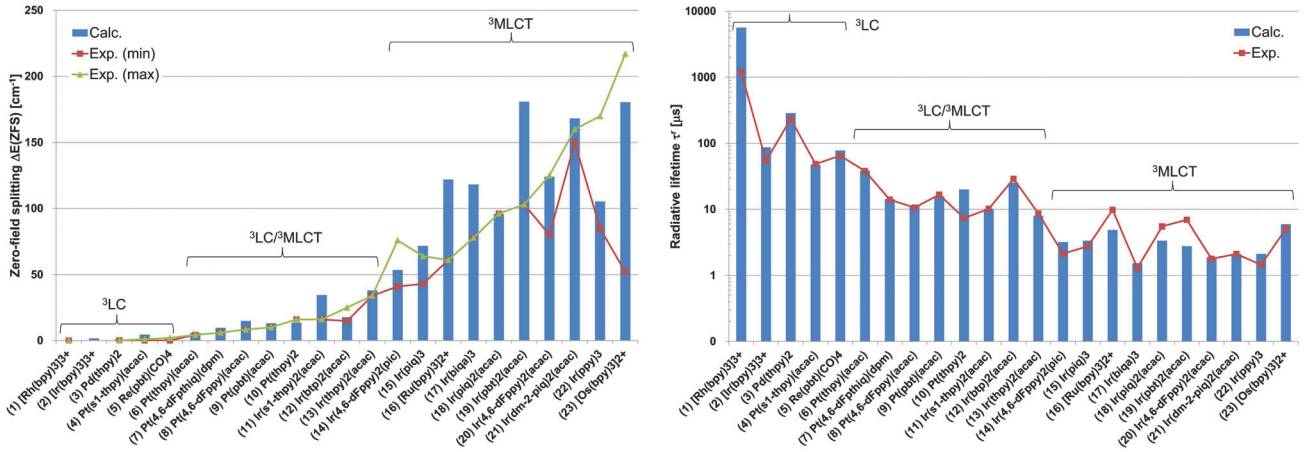

Fig. 1 Calculated ZFS (left, in cm^{-1}) and τ^r (right, in μs) at the COSMO + SOC-TDDFT level (blue bars) compared to experiment (symbols).

is promoted from an occupied metal d-orbital to the ligand π* orbitals. In an octahedral Ir(III) complex the highest occupied metal orbitals are triply degenerate (t_{2g}^6). Even if the symmetry is broken (non-identical ligands, Jahn–Teller distortion, . . .) the occupied d-orbitals will still be close in energy. This, in turn, means that the three d → π* excitations are close in energy. For square-planar d^8 complexes such as Pt(II), however, the occupied d-orbitals – and therefore excitations – are further apart in energy.

Although ZFS and finite $T_1 \rightarrow S_0$ transition probabilities both originate in SOC, the underlying mechanism is different. ZFS is a first order property, while the finite radiative lifetime is a second order property. The first-order term, in a degenerate perturbation approach to SOC, splits the three degenerate states of T_1 (*e.g.* $d_{xy} \rightarrow \pi^*$). The second order perturbation will mix these three substates with other singlet and triplet states. Here, the mixing occurs most effectively for the transitions from different d-orbitals to the same π* orbital (*e.g.* $d_{y^2-z^2} \rightarrow \pi^*$ or $d_{xz} \rightarrow \pi^*$). Other contributions are typically small. This is because (a) the spin–orbit interaction in ZORA Hamiltonian is a one-electron operator, (b) spin–orbit couplings between π electrons are very small and (c) spin–orbit couplings between the same d-orbitals are negligibly small. Consequently, singlet–triplet and triplet–triplet mixings occur most efficiently if the different d-orbitals involved in the MLCT transitions lie close in energy.

In summary, although the SOC constants are comparable for Ir and Pt, the mixing with other singlet and triplet states *via* SOC occurs more effectively for octahedral Ir(III) than for square-planar Pt(II) complexes. The stronger mixing results in a larger ZFS (as an effect of the second order term) and higher oscillator strengths, rendering a shorter radiative lifetime and possibly a higher quantum yield.

3.2 Impact of full spin–orbit and solvation effects

The impact of full spin–orbit and solvation effects on the calculated ZFS and τ^r will be discussed by comparing four different computational levels: pSOC-TDDFT/Gas, SOC-TDDFT/Gas, pSOC-TDDFT/COSMO, SOC-TDDFT/COSMO (the latter being our best theoretical approach). All the calculated values are summarized in Table S1 in the ESI.†

Solvation effect. Fig. 2 shows the differences of the ZFS values (left) and the ratios of the phosphorescent lifetimes (right) of gas phase calculations compared to the corresponding continuum

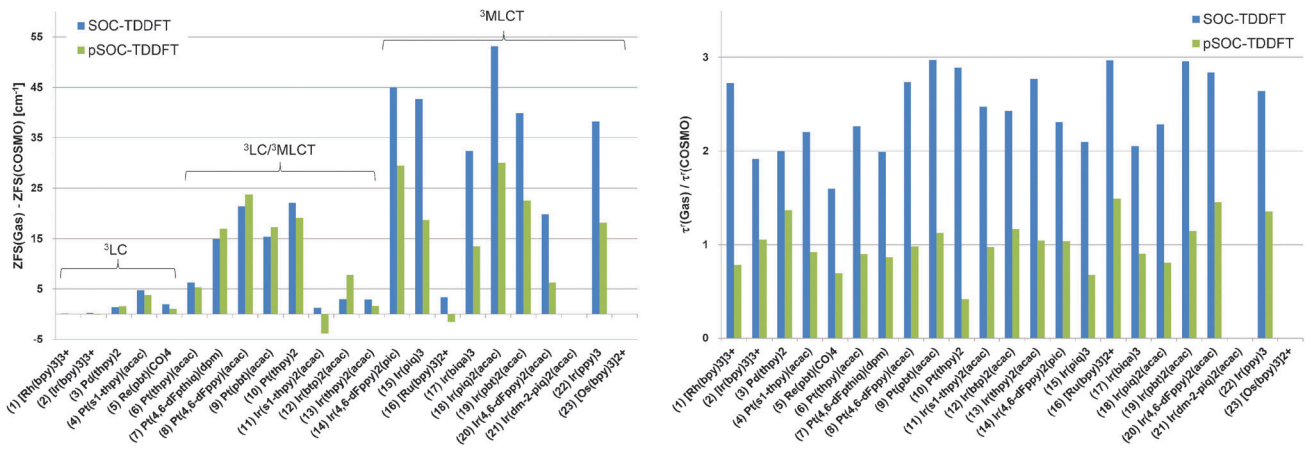

Fig. 2 Differences of ZFS values (left, in cm^{-1}) and ratios of phosphorescent lifetimes (right). Gas phase calculations are compared to the corresponding COSMO calculations both for SOC-TDDFT (blue bars) and pSOC-TDDFT (green bars).

solvation (COSMO) calculations, both for SOC-TDDFT (blue bars) and pSOC-TDDFT (green bars). The data of $Ir(dm\text{-}2\text{-}piq)_2(acac)$ (**21**) and $[Os(bpy)_3]^{2+}$ (**23**) are omitted from this figure because lower-symmetry geometries were not obtained for the gas phase calculations: C_2 *vs.* C_1 for **21**; D_3 *vs.* C_2 for **23**.

Excluding solvation effects in the SOC-TDDFT calculations increases both the ZFS and the radiative lifetime τ^r. On average, the gas phase ZFS is increased by 2, 11, and 34 cm^{-1} for the compounds with ^{3}LC, ^{3}LC/^{3}MLCT, and ^{3}MLCT character, respectively. τ^r is about 2 to 3 times longer in the gas phase than for COSMO calculations irrespective of the three classes of triplet emitting states.

With pSOC-TDDFT, gas phase ZFSs are also larger by 1, 11, and 17 cm^{-1} on average than values with solvation effects for the three different classes. However, solvation effects do not influence the pSOC-TDDFT radiative lifetimes much.

As noted before, the change of COSMO surface charges is not taken into account for the pSOC-TDDFT calculations. On the other hand, the COSMO surface charges are optimized for the excited states during the SOC-TDDFT calculations. Since the optimized COSMO surface charges will mainly affect the singlet excited states, these states will be lowered in energy, facilitating SOC. Perhaps more importantly, the optimized surface charges will stabilize more polarized states (*e.g.* ^{1}MLCT) compared to gas phase and unoptimized COSMO surface charge calculations. Therefore, the transition dipole moment is only strongly enhanced when COSMO is used in conjunction with SOC-TDDFT, resulting in reduced radiative lifetimes.

Perturbative *vs.* full spin–orbit coupling. Fig. 3 shows the differences of the ZFS values (left) and the ratios of the phosphorescent lifetimes (right) for pSOC-TDDFT calculations compared with the corresponding SOC-TDDFT calculations, both for COSMO (blue bars) and gas phase (green bars). For compounds with strong SOC, pSOC-TDDFT calculations will typically predict smaller ZFS than SOC-TDDFT since the perturbative method does not fully account for SOC.[24] Likewise, the radiative lifetime τ^r is longer at the pSOC-TDDFT level than at the SOC-TDDFT level, since the radiative lifetime of the triplet state depends on its mixing with singlet states through SOC.

Indeed, for compounds with ^{3}MLCT character (**14**)–(**23**) the calculated ZFS is smaller with the perturbative approach than with the full SOC approach by 23 cm^{-1} in the condensed phase and 45 cm^{-1} in the gas phase, on average. Likewise, for compounds (**14**)–(**23**), the calculated τ^r is higher by, on average, a factor of 3.3 (1.5) for the COSMO (gas phase) perturbative calculations compared to full SOC-TDDFT. The larger effect of full SOC on τ^r for COSMO than in the gas phase originates in the different treatment of COSMO surface charges for the full and perturbative SOC approaches. As explained above, the transition dipole moment of the emissive state is most strongly enhanced when the excited state surface charges are optimized as is the case only when COSMO is used with SOC-TDDFT. For the ^{3}LC and ^{3}LC/^{3}MLCT groups, the effect of full SOC compared to perturbative is much smaller for both ZFS and τ^r since these compounds have a smaller SOC.

In general the best agreement with experiment is found with SOC-TDDFT/COSMO for both ZFS and τ^r as visualized in Fig. S2 in the ESI.† For some complexes where SOC-TDDFT overestimates the ZFS, however, the pSOC-TDDFT values (most notably **16**, **17**, **19**) are in closer agreement with experiment. The better performance of the approximate pSOC-TDDFT approach in these cases may be fortuitous. Nevertheless, pSOC-TDDFT may be an alternative pragmatic approach with a reduced computational cost compared to SOC-TDDFT,[24] although the actual gain in computational efficiency of pSOC-TDDFT over SOC-TDDFT depends on the number of excitations (Table S2 in the ESI†).

The perturbative SOC approach allows one to analyze how singlet and triplet states from the SR picture are mixed in a robust manner compared to that of the full SOC approach.[24,30] Consequently, the singlet character of the three triplet substates can be analyzed also for larger-size molecules, yielding insight into the mechanisms that induce ZFS and enable radiative decay to the singlet ground state. Furthermore, SOC matrix elements (SOCMEs), which are important parameters

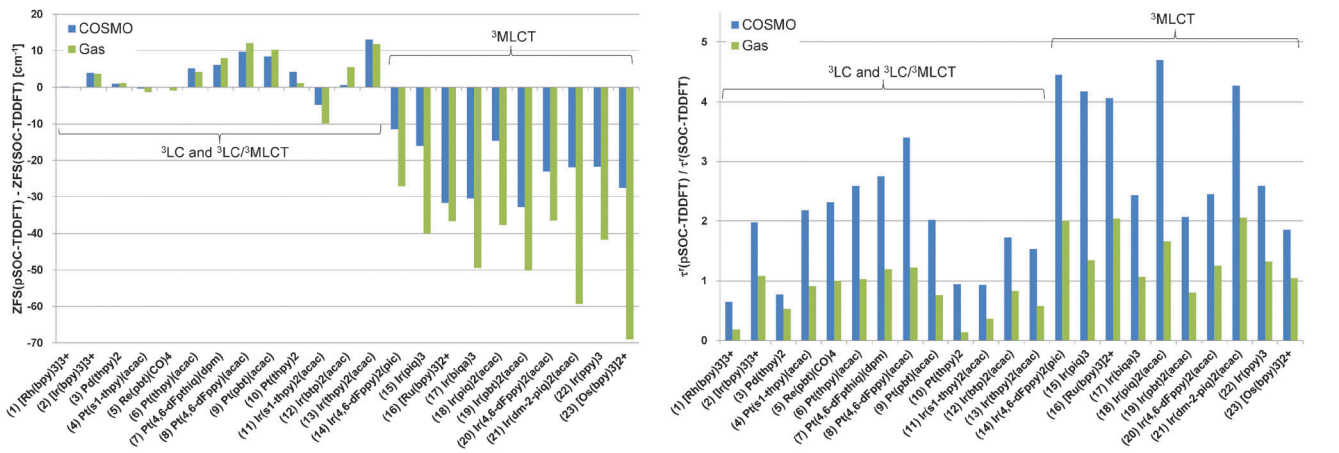

Fig. 3 Differences of ZFS values (left, in cm^{-1}) and ratios of phosphorescent lifetimes (right). pSOC-TDDFT calculations are compared to the corresponding SOC-TDDFT calculations both for COSMO (blue bars) and gas phase (green bars).

for calculating ISC rates,[40] can be calculated in the perturbative SOC approach.

3.3 Comparison with earlier theoretical studies: Ir(ppy)$_3$

Ir(ppy)$_3$ (**22**) has been previously studied with (perturbative) SOC approaches and TDDFT by Nozaki,[15] Jansson *et al.*,[16] Sasabe *et al.*,[4] Smith *et al.*,[20] and Younker and Dobbs.[25] The calculations by the former two groups use pseudopotentials on Ir and different perturbative SOC approaches. Nozaki's approach[15] is similar to the perturbative method used here, while a quadratic response method to treat SOC was employed in ref. 16. On the other hand, the latter three groups adopt the same (p)SOC-TDDFT method as was used in this study.[23,24] Table S3 in the ESI† compares our (p)SOC-TDDFT results in detail to the previous calculations based on the other perturbative approaches reported by Nozaki[15] and Jansson *et al.*[16]

Our calculations for pSOC-TDDFT/Gas, SOC-TDDFT/Gas and pSOC-TDDFT/COSMO at the T_1 geometry of Ir(ppy)$_3$ predict a mean radiative lifetime of 7.5 μs, 5.6 μs and 5.5 μs at 300 K, respectively. The radiative lifetimes calculated by Nozaki and Jansson *et al.* at T_1 structure compare well with our results (12.2 μs and 5.5 μs), when they are corrected for the refractive index of CH_2Cl_2 according to the Strickler–Berg relationship.[15,34] The experimentally measured radiative lifetime of Ir(ppy)$_3$ is 1.8 μs in CH_2Cl_2,[2] which is in excellent agreement with our SOC-TDDFT/COSMO value (2.1 μs). Here, it should be noted that our better agreement for the radiative lifetime may be again a result of including COSMO continuum solvation with optimized surface charges for the spin-mixed states in SOC-TDDFT. Our calculated ZFS values (except pSOC-TDDFT/COSMO) and that of Nozaki at the T_1 geometry are within the broad experimental range for ZFS, while our pSOC-TDDFT/COSMO value and the value reported by Jansson *et al.* are slightly lower. Our calculations and that of Nozaki reproduce an experimental trend for the splitting pattern of the triplet sublevels, which was observed for many d^6-type compounds with large ZFS: $\Delta E_{1,2} \ll \Delta E_{1,3}$ and k_1^r, $k_2^r \ll k_3^r$. The trend of this splitting pattern has been well rationalized previously by Nozaki[15] and others, using a localized model for a hypothetical M-LL unit considering that the excited state at T_1 structure is localized on one of the three ligands, *e.g.* as in the case for Ir(ppy)$_3$.[15,16]

Since the S_0 structure is C_3 symmetric, our gas phase (p)SOC-TDDFT calculations will predict the two highest substates of T_1 to be degenerate (E), in disagreement with the experimental splitting pattern. Interestingly, the calculated mean radiative lifetimes in the gas phase are much shorter at the S_0 geometry than at T_1 structures (1.2 μs and 1.7 μs for our pSOC-TDDFT and SOC-TDDFT calculations and 1.1 μs for the calculation by Jansson *et al.*). It seems to be natural to calculate phosphorescent properties at the T_1 structure assuming that the complex has enough time to relax to the T_1 equilibrium geometry before it phosphoresces. As Jansson *et al.* pointed out, however, the equilibrium geometry for the triplet state of Ir(ppy)$_3$ is a shallow minimum and therefore the triplet emitting state is perhaps better described by an intermediate between the singlet and triplet state structures.[16] Indeed, the same research group showed that their pSOC approach applied to S_0 geometries gives satisfactory results for the calculated mean radiative rates and lifetimes of various homoleptic and heteroleptic Ir compounds.[17,18,41,42] Likewise, the very recent results reported by Younker and Dobbs suggest that a good correlation with experimental results for nine Ir(III) emitters is obtained when performing the same gas phase pSOC-TDDFT calculations as in this study, but on the S_0 geometry at the BP86/TZ2P:TZP level.[25] Their approaches may work well for the Ir(III) complexes where emission arguably occurs from a singlet-state like geometry.[16–18,25,41,42]

4. Conclusions

Zero-field splitting (ZFS) and phosphorescent lifetime (τ^r) are important photophysical properties for the first triplet excited state of transition metal complexes. Understanding and tweaking these properties is crucially important to design more efficient compounds for applications in photovoltaic devices, photocatalysis, and OLEDs. The computational study of these compounds requires an accurate and efficient approach to treat the relativistic effects at play.

This paper offers a pragmatic approach for predicting photophysical properties of transition metal complexes. The recommended protocol is to first optimize the symmetry-lowered triplet state T_1 with a spin-unrestricted SR ZORA Hamiltonian, continuum solvation (COSMO) and the B3LYP functional. Subsequently, time-dependent density functional theory is used with the self-consistent ZORA spin–orbit Hamiltonian (SOC-TDDFT), COSMO and B3LYP. With this approach, good agreement was obtained with experimental ZFS and τ^r for 23 different compounds. Notable exceptions are an overestimated τ^r for $[Rh(bpy)_3]^{3+}$ (**1**), possibly due to competing non-radiative pathways, and $[Os(bpy)_3]^{2+}$ (**23**), where the higher D_3 symmetry needed to be considered for the ZFS to reflect the experimental geometry in a solid state matrix.

Both full spin–orbit and solvation effects are important for the accurate prediction of ZFS and τ^r. Especially, τ^r, a decisive property for efficient phosphors in OLEDs, is significantly affected by the use of COSMO solvation with optimized excited state surface charges for the spin-mixed excitations in SOC-TDDFT. Our (perturbative) SOC-TDDFT calculations compare well to previous theoretical studies employing other perturbative SOC approaches for a typical Ir complex when the same conditions are considered. The best agreement with experiment is again achieved by combining SOC-TDDFT with COSMO.

Modifying ligands with electronic-donating or -withdrawing groups may strongly influence the electronic properties of both the ground and the ^{3}MLCT state, and thereby the emission properties.[3] *In silico* screening of suitable candidate organometallic complexes for high-efficiency OLED applications can thus be achieved by applying the computational chemistry protocol outlined in Section 2 to accurately and efficiently estimate the phosphorescent lifetime of a set of compounds.

Acknowledgements

Stan van Gisbergen (SCM) is thanked for useful discussions.

Notes and references

1 *Highly Efficient OLEDs with Phosphorescent Materials*, ed. H. Yersin, Wiley-VCH, Weinheim, 2008.
2 H. Yersin, A. F. Rausch, R. Czerwieniec, T. Hofbeck and T. Fischer, *Coord. Chem. Rev.*, 2011, **255**, 2622.
3 A. R. G. Smith, M. J. Riley, P. L. Burn, I. R. Gentle, S.-C. Lo and B. J. Powell, *Inorg. Chem.*, 2012, **51**, 2821.
4 H. Sasabe, J. Takamatsu, T. Motoyama, S. Watanabe, G. Wagenblast, N. Langer, O. Molt, E. Fuchs, C. Lennartz and J. Kido, *Adv. Mater.*, 2010, **22**, 5003.
5 M. Grätzel, *Inorg. Chem.*, 2005, **44**, 6841; J. Wang, H. Li, N.-N. Ma, L.-K. Yan and Z.-M. Su, *Dyes Pigm.*, 2013, **99**, 440.
6 M. H. Keefe, K. D. Benkstein and J. T. Hupp, *Coord. Chem. Rev.*, 2000, **205**, 201; K. K.-W. Lo, M.-W. Louie and K. Y. Zhang, *Coord. Chem. Rev.*, 2010, **254**, 2603.
7 T. P. Yoon, M. A. Ischay and J. Du, *Nat. Chem.*, 2010, **2**, 527; J. M. R. Narayanam and C. R. J. Stephenson, *Chem. Soc. Rev.*, 2011, **40**, 102.
8 P. Pyykkö, *Adv. Quantum Chem.*, 1978, **11**, 353; K. S. Pitzer, *Acc. Chem. Res.*, 1979, **12**, 271; E. J. Baerends, W. H. E. Schwarz, P. Schwerdtfeger and J. G. Snijders, *J. Phys. B: At., Mol. Opt. Phys.*, 1990, **23**, 3225; N. Kaltsoyannis, *J. Chem. Soc., Dalton Trans.*, 1997, 1.
9 B. O. Roos and P.-Å. Malmqvist, *Adv. Quantum Chem.*, 2004, **47**, 37; F. Neese, T. Petrenko, D. Ganyushin and G. Olbrich, *Coord. Chem. Rev.*, 2007, **251**, 288; P. Pyykkö, *Annu. Rev. Phys. Chem.*, 2012, **63**, 45.
10 M. A. Baldo, D. F. O'Brien, Y. You, A. Shoustikov, S. Sibley, M. E. Thompson and S. R. Forrest, *Nature*, 1998, **395**, 151.
11 M. A. Baldo, S. Lamansky, P. E. Burrows, M. E. Thompson and S. R. Forrest, *Appl. Phys. Lett.*, 1999, **75**, 4.
12 L. Xiao, Z. Chen, B. Qu, J. Luo, S. Kong, Q. Gong and J. Kido, *Adv. Mater.*, 2011, **23**, 926.
13 C. Adachi, M. A. Baldo, M. E. Thompson and S. R. Forrest, *J. Appl. Phys.*, 2001, **90**, 5048.
14 P. J. Hay, *J. Phys. Chem. A*, 2002, **106**, 1634.
15 K. Nozaki, *J. Chin. Chem. Soc.*, 2006, **53**, 101.
16 E. Jansson, B. Minaev, S. Schrader and H. Ågren, *Chem. Phys.*, 2007, **333**, 157.
17 B. Minaev, H. Ågren and F. De Angelis, *Chem. Phys.*, 2009, **358**, 245.
18 B. Minaev, V. Minaeva and H. Ågren, *J. Phys. Chem. A*, 2009, **113**, 726.
19 A. R. G. Smith, M. J. Riley, S.-C. Lo, P. L. Burn, I. R. Gentle and B. J. Powell, *Phys. Rev. B: Condens. Matter Mater. Phys.*, 2011, **83**, 041105(R).
20 A. R. G. Smith, P. L. Burn and B. J. Powell, *ChemPhysChem*, 2011, **12**, 2429.
21 E. van Lenthe, E. J. Baerends and J. G. Snijders, *J. Chem. Phys.*, 1993, **99**, 4597.
22 E. van Lenthe, E. J. Baerends and J. G. Snijders, *J. Chem. Phys.*, 1994, **101**, 9783.
23 F. Wang, T. Ziegler, E. van Lenthe, S. J. A. van Gisbergen and E. J. Baerends, *J. Chem. Phys.*, 2005, **122**, 204103.
24 F. Wang and T. Ziegler, *J. Chem. Phys.*, 2005, **123**, 154102.
25 J. M. Younker and K. D. Dobbs, *J. Phys. Chem. C*, 2013, **117**, 25714.
26 E. J. Baerends, T. Ziegler, J. Autschbach, D. Bashford, A. Bérces, F. M. Bickelhaupt, C. Bo, P. M. Boerrigter, L. Cavallo, D. P. Chong, L. Deng, R. M. Dickson, D. E. Ellis, M. van Faassen, L. Fan, T. H. Fischer, C. Fonseca Guerra, M. Franchini, A. Ghysels, A. Giammona, S. J. A. van Gisbergen, A. W. Götz, J. A. Groeneveld, O. V. Gritsenko, M. Grüning, S. Gusarov, F. E. Harris, P. van den Hoek, C. R. Jacob, H. Jacobsen, L. Jensen, J. W. Kaminski, G. van Kessel, F. Kootstra, A. Kovalenko, M. V. Krykunov, E. van Lenthe, D. A. McCormack, A. Michalak, M. Mitoraj, S. M. Morton, J. Neugebauer, V. P. Nicu, L. Noodleman, V. P. Osinga, S. Patchkovskii, M. Pavanello, P. H. T. Philipsen, D. Post, C. C. Pye, W. Ravenek, J. I. Rodríguez, P. Ros, P. R. T. Schipper, G. Schreckenbach, J. S. Seldenthuis, M. Seth, J. G. Snijders, M. Solà, M. Swart, D. Swerhone, G. te Velde, P. Vernooijs, L. Versluis, L. Visscher, O. Visser, F. Wang, T. A. Wesolowski, E. M. van Wezenbeek, G. Wiesenekker, S. K. Wolff, T. K. Woo and A. L. Yakovlev, *ADF2013.01b, SCM, Theoretical Chemistry*, Vrije Universiteit, Amsterdam, The Netherlands, http://www.scm.com.
27 C. Fonseca Guerra, J. G. Snijders, G. te Velde and E. J. Baerends, *Theor. Chem. Acc.*, 1998, **99**, 391; G. te Velde, F. M. Bickelhaupt, E. J. Baerends, C. Fonseca Guerra, S. J. A. van Gisbergen, J. G. Snijders and T. Ziegler, *J. Comput. Chem.*, 2001, **22**, 931.
28 A. D. Becke, *J. Chem. Phys.*, 1993, **98**, 5648; C. Lee, W. Yang and R. G. Parr, *Phys. Rev. B: Condens. Matter Mater. Phys.*, 1988, **37**, 785; S. H. Vosko, L. Wilk and M. Nusair, *Can. J. Phys.*, 1980, **58**, 1200; P. J. Stephens, F. J. Devlin, C. F. Chabalowski and M. J. Frisch, *J. Phys. Chem.*, 1994, **98**, 11623.
29 E. van Lenthe and E. J. Baerends, *J. Comput. Chem.*, 2003, **24**, 1142.
30 F. Wang and T. Ziegler, *J. Chem. Phys.*, 2005, **123**, 194102.
31 M. Franchini, P. H. T. Philipsen and L. Visscher, *J. Comput. Chem.*, 2013, **34**, 1819.
32 K. Nozaki, K. Takamori, Y. Nakatsugawa and T. Ohno, *Inorg. Chem.*, 2006, **45**, 6161.
33 C. C. Pye and T. Ziegler, *Theor. Chem. Acc.*, 1999, **101**, 396.
34 S. J. Strickler and R. A. Berg, *J. Chem. Phys.*, 1962, **37**, 814.
35 E. Krausz, J. Higgins and H. Riesen, *Inorg. Chem.*, 1993, **32**, 4053.
36 H. Ishida, S. Tobita, Y. Hasegawa, R. Katoh and K. Nozaki, *Coord. Chem. Rev.*, 2010, **254**, 2449.
37 D. E. Lacky, B. J. Pankuch and G. A. Crosby, *J. Phys. Chem.*, 1980, **84**, 2068.
38 H. Yersin, W. Humbs and J. Strasser, *Top. Curr. Chem.*, 1997, **191**, 153.
39 E. M. Kober, J. V. Caspar, R. S. Lumpkin and T. J. Meyer, *J. Phys. Chem.*, 1986, **90**, 3722.
40 C. M. Marian, *Wiley Interdiscip. Rev.: Comput. Mol. Sci.*, 2012, **2**, 187.
41 B. Minaev, G. Baryshnikov and H. Ågren, *Phys. Chem. Chem. Phys.*, 2014, **16**, 1719.
42 X. Li, B. Minaev, H. Ågren and H. Tian, *J. Phys. Chem. C*, 2011, **115**, 20724; X. Li, B. Minaev, H. Ågren and H. Tian, *Eur. J. Inorg. Chem.*, 2011, 2517.

